

Handbook of Time Series Analysis

Recent Theoretical Developments and Applications

Edited by
Björn Schelter, Matthias Winterhalder,
and Jens Timmer



WILEY-
VCH

WILEY-VCH Verlag GmbH & Co. KGaA

on Theory

17 Granger Causality: Basic Theory and Application to Neuroscience

Mingzhou Ding, Yonghong Chen, and Steven L. Bressler

Multielectrode neurophysiological recordings produce massive quantities of data. Multivariate time series analysis provides the basic framework for analyzing the patterns of neural interactions in these data. It has long been recognized that neural interactions are directional. Being able to assess the directionality of neuronal interactions is thus a highly desired capability for understanding the cooperative nature of neural computation. Research over the last few years has shown that Granger causality is a key technique to furnish this capability. The main goal of this chapter is to provide an expository introduction to the concept of Granger causality. Mathematical frameworks for both the bivariate Granger causality and conditional Granger causality are developed in detail, with particular emphasis on their spectral representations. The technique is demonstrated in numerical examples where the exact answers of causal influences are known. It is then applied to analyze multichannel local field potentials recorded from monkeys performing a visuomotor task. Our results are shown to be physiologically interpretable and yield new insights into the dynamical organization of large-scale oscillatory cortical networks.

17.1 Introduction

In neuroscience, as in many other fields of science and engineering, signals of interest are often collected in the form of multiple simultaneous time series. To evaluate the statistical interdependence among these signals, one calculates cross-correlation functions in the time domain and ordinary coherence functions in the spectral domain. However, in many situations of interest, symmetric¹ measures like ordinary coherence are not completely satisfactory, and further dissection of the interaction patterns among the recorded signals is required to parcel out effective functional connectivity in complex networks. Recent work has begun to consider the causal influence one neural time series can exert on another. The basic idea can be traced back to Wiener [1] who conceived the notion that, if the prediction of one time series could be improved by incorporating the knowledge

¹ Here by symmetric we mean that, when A is coherent with B, B is equally coherent with A.

of a second one, then the second series is said to have a causal influence on the first. Wiener's idea lacks the machinery for practical implementation. Granger later formalized the prediction idea in the context of linear regression models [2]. Specifically, if the variance of the autoregressive prediction error of the first time series at the present time is reduced by inclusion of past measurements from the second time series, then the second time series is said to have a causal influence on the first one. The roles of the two time series can be reversed to address the question of causal influence in the opposite direction. From this definition it is clear that the flow of time plays a vital role in allowing inferences to be made about directional causal influences from time series data. The interaction discovered in this way may be reciprocal or it may be unidirectional.

Two additional developments of Granger's causality idea are important. First, for three or more simultaneous time series, the causal relation between any two of the series may be direct, may be mediated by a third one, or may be a combination of both. This situation can be addressed by the technique of conditional Granger causality. Second, natural time series, including ones from economics and neurobiology, contain oscillatory aspects in specific frequency bands. It is thus desirable to have a spectral representation of causal influence. Major progress in this direction has been made by Geweke [3, 4] who found a novel time series decomposition technique that expresses the time domain Granger causality in terms of its frequency content. In this chapter we review the essential mathematical elements of Granger causality with special emphasis on its spectral decomposition. We then discuss practical issues concerning how to estimate such measures from time series data. Simulations are used to illustrate the theoretical concepts. Finally, we apply the technique to analyze the dynamics of a large-scale sensorimotor network in the cerebral cortex during cognitive performance. Our result demonstrates that, for a well designed experiment, a carefully executed causality analysis can reveal insights that are not possible with other techniques.

17.2 Bivariate Time Series and Pairwise Granger Causality

Our exposition in this and the next section follows closely that of Geweke [3, 4]. To avoid excessive mathematical complexity we develop the analysis framework for two time series. The framework can be generalized to two sets of time series [3].

17.2.1 Time Domain Formulation

Consider two stochastic processes X_t and Y_t . Assume that they are jointly stationary. Individually, under fairly general conditions, each process admits an autoregressive representation

Joint

when
covaThe
and
and
betwwhen
initic
theyC
autor
of Σ_2
previ
 Σ_2 is
influIt is c
0 whIt
plain

$$X_t = \sum_{j=1}^{\infty} a_{1j} X_{t-j} + \epsilon_{1t}, \quad \text{var}(\epsilon_{1t}) = \Sigma_1, \quad (17.1)$$

$$Y_t = \sum_{j=1}^{\infty} d_{1j} Y_{t-j} + \eta_{1t}, \quad \text{var}(\eta_{1t}) = \Gamma_1. \quad (17.2)$$

Jointly, they are represented as

$$X_t = \sum_{j=1}^{\infty} a_{2j} X_{t-j} + \sum_{j=1}^{\infty} b_{2j} Y_{t-j} + \epsilon_{2t}, \quad (17.3)$$

$$Y_t = \sum_{j=1}^{\infty} c_{2j} X_{t-j} + \sum_{j=1}^{\infty} d_{2j} Y_{t-j} + \eta_{2t}, \quad (17.4)$$

where the noise terms are uncorrelated over time and their contemporaneous covariance matrix is

$$\Sigma = \begin{pmatrix} \Sigma_2 & \Upsilon_2 \\ \Upsilon_2 & \Gamma_2 \end{pmatrix}. \quad (17.5)$$

The entries are defined as $\Sigma_2 = \text{var}(\epsilon_{2t})$, $\Gamma_2 = \text{var}(\eta_{2t})$, $\Upsilon_2 = \text{cov}(\epsilon_{2t}, \eta_{2t})$. If X_t and Y_t are independent, then $\{b_{2j}\}$ and $\{c_{2j}\}$ are uniformly zero, $\Upsilon_2 = 0$, $\Sigma_1 = \Sigma_2$ and $\Gamma_1 = \Gamma_2$. This observation motivates the definition of total interdependence between X_t and Y_t as

$$F_{X,Y} = \ln \frac{\Sigma_1 \Gamma_1}{|\Sigma|}, \quad (17.6)$$

where $|\cdot|$ denotes the determinant of the enclosed matrix. According to this definition, $F_{X,Y} = 0$ when the two time series are independent, and $F_{X,Y} > 0$ when they are not.

Consider Eqs. (17.1) and (17.3). The value of Σ_1 measures the accuracy of the autoregressive prediction of X_t based on its previous values, whereas the value of Σ_2 represents the accuracy of predicting the present value of X_t based on the previous values of both X_t and Y_t . According to Wiener [1] and Granger [2], if Σ_2 is less than Σ_1 in some suitable statistical sense, then Y_t is said to have a causal influence on X_t . We quantify this causal influence by

$$F_{Y \rightarrow X} = \ln \frac{\Sigma_1}{\Sigma_2}. \quad (17.7)$$

It is clear that $F_{Y \rightarrow X} = 0$ when there is no causal influence from Y to X and $F_{Y \rightarrow X} > 0$ when there is. Similarly, one can define causal influence from X to Y as

$$F_{X \rightarrow Y} = \ln \frac{\Gamma_1}{\Gamma_2}. \quad (17.8)$$

It is possible that the interdependence between X_t and Y_t cannot be fully explained by their interactions. The remaining interdependence is captured by Υ_2 ,

the covariance between ϵ_{2t} and η_{2t} . This interdependence is referred to as instantaneous causality and is characterized by

$$F_{X,Y} = \ln \frac{\Sigma_2 \Gamma_2}{|\Sigma|}. \quad (17.9)$$

When Υ_2 is zero, $F_{X,Y}$ is also zero. When Υ_2 is not zero, $F_{X,Y} > 0$.

The above definitions imply that

$$F_{X,Y} = F_{X \rightarrow Y} + F_{Y \rightarrow X} + F_{X,Y}. \quad (17.10)$$

Thus we decompose the total interdependence between the two time series X_t and Y_t into three components: two directional causal influences due to their interaction patterns, and the instantaneous causality due to factors possibly exogenous to the (X, Y) system, e.g., a common driving input.

17.2.2 Frequency Domain Formulation

To begin we define the lag operator L to be $LX_t = X_{t-1}$. Rewrite Eqs. (17.3) and (17.4) in terms of the lag operator

$$\begin{pmatrix} a_2(L) & b_2(L) \\ c_2(L) & d_2(L) \end{pmatrix} \begin{pmatrix} X_t \\ Y_t \end{pmatrix} = \begin{pmatrix} \epsilon_{2t} \\ \eta_{2t} \end{pmatrix}, \quad (17.11)$$

where $a_2(0) = 1$, $b_2(0) = 0$, $c_2(0) = 0$, $d_2(0) = 1$. Fourier transforming both sides of Eq. (17.11) leads to

$$\begin{pmatrix} a_2(\omega) & b_2(\omega) \\ c_2(\omega) & d_2(\omega) \end{pmatrix} \begin{pmatrix} X(\omega) \\ Y(\omega) \end{pmatrix} = \begin{pmatrix} E_x(\omega) \\ E_y(\omega) \end{pmatrix}, \quad (17.12)$$

where the components of the coefficient matrix $\mathbf{A}(\omega)$ are

$$\begin{aligned} a_2(\omega) &= 1 - \sum_{j=1}^{\infty} a_{2j} e^{-i\omega j}, & b_2(\omega) &= - \sum_{j=1}^{\infty} b_{2j} e^{-i\omega j}, \\ c_2(\omega) &= - \sum_{j=1}^{\infty} c_{2j} e^{-i\omega j}, & d_2(\omega) &= 1 - \sum_{j=1}^{\infty} d_{2j} e^{-i\omega j}. \end{aligned}$$

Recasting Eq. (17.12) into the transfer function format we obtain

$$\begin{pmatrix} X(\omega) \\ Y(\omega) \end{pmatrix} = \begin{pmatrix} H_{xx}(\omega) & H_{xy}(\omega) \\ H_{yx}(\omega) & H_{yy}(\omega) \end{pmatrix} \begin{pmatrix} E_x(\omega) \\ E_y(\omega) \end{pmatrix}, \quad (17.13)$$

where the transfer function is $\mathbf{H}(\omega) = \mathbf{A}^{-1}(\omega)$ whose components are

$$\begin{aligned} H_{xx}(\omega) &= \frac{1}{\det \mathbf{A}} d_2(\omega), & H_{xy}(\omega) &= - \frac{1}{\det \mathbf{A}} b_2(\omega), \\ H_{yx}(\omega) &= - \frac{1}{\det \mathbf{A}} c_2(\omega), & H_{yy}(\omega) &= \frac{1}{\det \mathbf{A}} a_2(\omega). \end{aligned} \quad (17.14)$$

After

when
T
indep
two
of towhen
to se
follow

when

The c
ence.
T
in theIt is i
stant
due t
of Eq
the ir
drive
only
comp
for de
W
to dif
that r
term
and it

After proper ensemble averaging we have the spectral matrix

$$\mathbf{S}(\omega) = \mathbf{H}(\omega)\boldsymbol{\Sigma}\mathbf{H}^*(\omega), \quad (17.15)$$

where * denotes the complex conjugate and matrix transpose.

The spectral matrix contains cross-spectra and auto-spectra. If X_t and Y_t are independent, then the cross-spectra are zero and $|\mathbf{S}(\omega)|$ equals the product of two auto-spectra. This observation motivates the spectral domain representation of total interdependence between X_t and Y_t as

$$f_{X,Y}(\omega) = \ln \frac{S_{xx}(\omega)S_{yy}(\omega)}{|\mathbf{S}(\omega)|}, \quad (17.16)$$

where $|\mathbf{S}(\omega)| = S_{xx}(\omega)S_{yy}(\omega) - S_{xy}(\omega)S_{yx}(\omega)$ and $S_{yx}(\omega) = S_{xy}^*(\omega)$. It is easy to see that this decomposition of interdependence is related to coherence by the following relation

$$f_{X,Y}(\omega) = -\ln(1 - C(\omega)), \quad (17.17)$$

where coherence is defined as

$$C(\omega) = \frac{|S_{xy}(\omega)|^2}{S_{xx}(\omega)S_{yy}(\omega)}.$$

The coherence defined in this way is sometimes referred to as the squared coherence.

To obtain the frequency decomposition of the time domain causality defined in the previous section, we look at the auto-spectrum of X_t

$$S_{xx}(\omega) = H_{xx}(\omega)\boldsymbol{\Sigma}_2 H_{xx}^*(\omega) + 2\Upsilon_2 \operatorname{Re}(H_{xx}(\omega)H_{xy}^*(\omega)) + H_{xy}(\omega)\Gamma_2 H_{xy}^*(\omega). \quad (17.18)$$

It is instructive to consider the case where $\Upsilon_2 = 0$. In this case there is no instantaneous causality and the interdependence between X_t and Y_t is entirely due to their interactions through the regression terms on the right-hand sides of Eqs. (17.3) and (17.4). The spectrum has two terms. The first term, viewed as the intrinsic part, involves only the variance of ϵ_{2t} , which is the noise term that drives the X_t time series. The second term, viewed as the causal part, involves only the variance of η_{2t} , which is the noise term that drives Y_t . This power decomposition into an "intrinsic" term and a "causal" term will become important for defining a measure for spectral domain causality.

When Υ_2 is not zero it becomes harder to attribute the power of the X_t series to different sources. Here we consider a transformation introduced by Geweke [3] that removes the cross term and makes the identification of an intrinsic power term and a causal power term possible. The procedure is called normalization and it consists of left multiplying

$$\mathbf{P} = \begin{pmatrix} 1 & 0 \\ -\Upsilon_2 & 1 \\ \boldsymbol{\Sigma}_2 & \end{pmatrix} \quad (17.19)$$

on both sides of Eq. (17.12). The result is

$$\begin{pmatrix} a_2(\omega) & b_2(\omega) \\ c_3(\omega) & d_3(\omega) \end{pmatrix} \begin{pmatrix} X(\omega) \\ Y(\omega) \end{pmatrix} = \begin{pmatrix} E_x(\omega) \\ \tilde{E}_y(\omega) \end{pmatrix}, \quad (17.20)$$

where $c_3(\omega) = c_2(\omega) - \frac{\gamma_2}{\Sigma_2} a_2(\omega)$, $d_3(\omega) = d_2(\omega) - \frac{\gamma_2}{\Sigma_2} b_2(\omega)$, $\tilde{E}_y(\omega) = E_y(\omega) - \frac{\gamma_2}{\Sigma_2} E_x(\omega)$. The new transfer function $\tilde{H}(\omega)$ for Eq. (17.20) is the inverse of the new coefficient matrix $\tilde{A}(\omega)$

$$\tilde{H}(\omega) = \begin{pmatrix} \tilde{H}_{xx}(\omega) & \tilde{H}_{xy}(\omega) \\ \tilde{H}_{yx}(\omega) & \tilde{H}_{yy}(\omega) \end{pmatrix} = \frac{1}{\det \tilde{A}} \begin{pmatrix} d_3(\omega) & -b_2(\omega) \\ -c_3(\omega) & a_2(\omega) \end{pmatrix}. \quad (17.21)$$

Since $\det \tilde{A} = \det A$ we have

$$\begin{aligned} \tilde{H}_{xx}(\omega) &= H_{xx}(\omega) + \frac{\gamma_2}{\Sigma_2} H_{xy}(\omega), & \tilde{H}_{xy}(\omega) &= H_{xy}(\omega), \\ \tilde{H}_{yx}(\omega) &= H_{yx}(\omega) + \frac{\gamma_2}{\Sigma_2} H_{xx}(\omega), & \tilde{H}_{yy}(\omega) &= H_{yy}(\omega). \end{aligned} \quad (17.22)$$

From the construction it is easy to see that E_x and \tilde{E}_y are uncorrelated, that is, $\text{cov}(E_x, \tilde{E}_y) = 0$. The variance of the noise term for the normalized Y_t equation is $\tilde{\Gamma}_2 = \Gamma_2 - \frac{\gamma_2^2}{\Sigma_2}$. From Eq. (17.20), following the same steps that lead to Eq. (17.18), the spectrum of X_t is found to be

$$S_{xx}(\omega) = \tilde{H}_{xx}(\omega) \Sigma_2 \tilde{H}_{xx}^*(\omega) + H_{xy}(\omega) \tilde{\Gamma}_2 H_{xy}^*(\omega). \quad (17.23)$$

Here the first term is interpreted as the intrinsic power and the second term as the causal power of X_t due to Y_t . This is an important relation because it explicitly identifies that portion of the total power of X_t at frequency ω that is contributed by Y_t . Based on this interpretation we define the causal influence from Y_t to X_t at frequency ω as

$$f_{Y \rightarrow X}(\omega) = \ln \frac{S_{xx}(\omega)}{\tilde{H}_{xx}(\omega) \Sigma_2 \tilde{H}_{xx}^*(\omega)}. \quad (17.24)$$

Note that this definition of causal influence is expressed in terms of the intrinsic power rather than the causal power. It is expressed in this way so that the causal influence is zero when the causal power is zero (i.e., the intrinsic power equals the total power), and increases as the causal power increases (i.e., the intrinsic power decreases).

By taking the transformation matrix as

$$\begin{pmatrix} 1 & -\gamma_2/\Gamma_2 \\ 0 & 1 \end{pmatrix} \quad (17.25)$$

and performing the same analysis, we get the causal influence from X_t to Y_t

$$f_{X \rightarrow Y}(\omega) = \ln \frac{S_{yy}(\omega)}{\tilde{H}_{yy}(\omega) \Gamma_2 \tilde{H}_{yy}^*(\omega)}, \quad (17.26)$$

when
B

we a
anal

We c
some
phys.
It
relate

The e
proce

17.3

For tl
duce
tation
sis w
exam
differ
from
input
define
intera
time
delay
ries. I

where $\hat{H}_{yy}(\omega) = H_{yy}(\omega) + \frac{\gamma^2}{\Gamma_2} H_{yx}(\omega)$.

By defining the spectral decomposition of instantaneous causality as [5]

$$f_{X,Y}(\omega) = \ln \frac{(\bar{H}_{xx}(\omega) \Sigma_2 \bar{H}_{xx}^*(\omega)) (\hat{H}_{yy}(\omega) \Gamma_2 \hat{H}_{yy}^*(\omega))}{|S(\omega)|}, \quad (17.27)$$

we achieve a spectral domain expression for the total interdependence that is analogous to Eq. (17.10) in the time domain, namely

$$f_{X,Y}(\omega) = f_{X \rightarrow Y}(\omega) + f_{Y \rightarrow X}(\omega) + f_{X,Y}(\omega). \quad (17.28)$$

We caution that the spectral instantaneous causality may become negative for some frequencies in certain situations and may not have a readily interpretable physical meaning.

It is important to note that, under general conditions, these spectral measures relate to the time domain measures as

$$\begin{aligned} F_{Y,X} &= \frac{1}{2\pi} \int_{-\pi}^{\pi} f_{Y,X}(\omega) d\omega, \\ F_{Y \rightarrow X} &= \frac{1}{2\pi} \int_{-\pi}^{\pi} f_{Y \rightarrow X}(\omega) d\omega, \\ F_{X \rightarrow Y} &= \frac{1}{2\pi} \int_{-\pi}^{\pi} f_{X \rightarrow Y}(\omega) d\omega, \\ F_{Y,X} &= \frac{1}{2\pi} \int_{-\pi}^{\pi} f_{Y,X}(\omega) d\omega. \end{aligned} \quad (17.29)$$

The existence of these equalities gives credence to the spectral decomposition procedures described above.

17.3 Trivariate Time Series and Conditional Granger Causality

For three or more time series one can perform a pairwise analysis and thus reduce the problem to a bivariate problem. This approach has some inherent limitations. For example, for the two coupling schemes in Fig. 17.1, a pairwise analysis will give the same patterns of connectivity like that in Fig. 17.1(b). Another example involves three processes where one process drives the other two with differential time delays. A pairwise analysis would indicate a causal influence from the process that receives an early input to the process that receives a late input. To disambiguate these situations requires additional measures. Here we define conditional Granger causality which has the ability to resolve whether the interaction between two time series is direct or is mediated by another recorded time series and whether the causal influence is simply due to differential time delays in their respective driving inputs. Our development is for three time series. The framework can be generalized to three sets of time series [4].

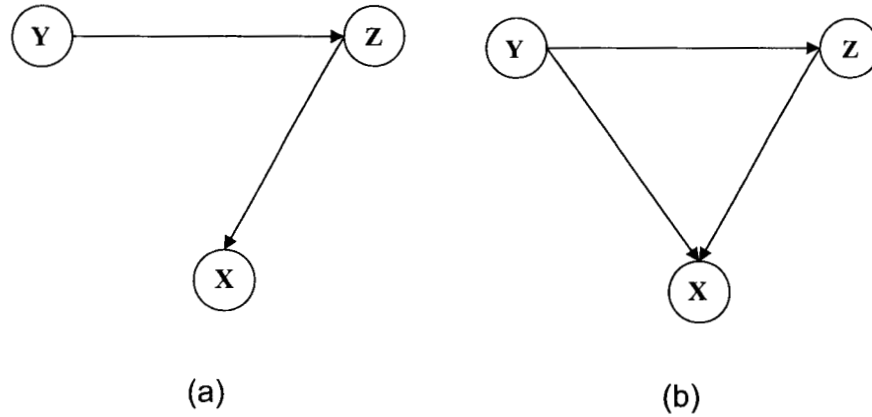


Fig. 17.1: Two distinct patterns of connectivity among three time series. A pairwise causality analysis cannot distinguish these two patterns.

17.3.1 Time Domain Formulation

Consider three stochastic processes X_t , Y_t and Z_t . Suppose that a pairwise analysis reveals a causal influence from Y_t to X_t . To examine whether this influence has a direct component (Fig. 17.1(b)) or is mediated entirely by Z_t (Fig. 17.1(a)) we carry out the following procedure. First, let the joint autoregressive representation of X_t and Z_t be

$$X_t = \sum_{j=1}^{\infty} a_{3j} X_{t-j} + \sum_{j=1}^{\infty} b_{3j} Z_{t-j} + \epsilon_{3t}, \quad (17.30)$$

$$Z_t = \sum_{j=1}^{\infty} c_{3j} X_{t-j} + \sum_{j=1}^{\infty} d_{3j} Z_{t-j} + \gamma_{3t}, \quad (17.31)$$

where the covariance matrix of the noise terms is

$$\Sigma_3 = \begin{pmatrix} \Sigma_3 & \Upsilon_3 \\ \Upsilon_3 & \Gamma_3 \end{pmatrix}. \quad (17.32)$$

Next we consider the joint autoregressive representation of all the three processes X_t , Y_t , and Z_t

$$X_t = \sum_{j=1}^{\infty} a_{4j} X_{t-j} + \sum_{j=1}^{\infty} b_{4j} Y_{t-j} + \sum_{j=1}^{\infty} c_{4j} Z_{t-j} + \epsilon_{4t}, \quad (17.33)$$

$$Y_t = \sum_{j=1}^{\infty} d_{4j} X_{t-j} + \sum_{j=1}^{\infty} e_{4j} Y_{t-j} + \sum_{j=1}^{\infty} g_{4j} Z_{t-j} + \eta_{4t}, \quad (17.34)$$

$$Z_t = \sum_{j=1}^{\infty} u_{4j} X_{t-j} + \sum_{j=1}^{\infty} v_{4j} Y_{t-j} + \sum_{j=1}^{\infty} w_{4j} Z_{t-j} + \gamma_{4t}, \quad (17.35)$$

where the covariance matrix of the noise terms is

$$\Sigma_4 = \begin{pmatrix} \Sigma_{xx} & \Sigma_{xy} & \Sigma_{xz} \\ \Sigma_{yx} & \Sigma_{yy} & \Sigma_{yz} \\ \Sigma_{zx} & \Sigma_{zy} & \Sigma_{zz} \end{pmatrix}.$$

From these two sets of equations we define the Granger causality from Y_t to X_t conditional on Z_t to be

$$F_{Y \rightarrow X|Z} = \ln \frac{\Sigma_3}{\Sigma_{xx}}. \quad (17.36)$$

The intuitive meaning of this definition is quite clear. When the causal influence from Y_t to X_t is entirely mediated by Z_t (Fig. 17.1(a)), $\{b_{4j}\}$ is uniformly zero, and $\Sigma_{xx} = \Sigma_3$. Thus, we have $F_{Y \rightarrow X|Z} = 0$, meaning that no further improvement in the prediction of X_t can be expected by including past measurements of Y_t . On the other hand, when there is still a direct component from Y_t to X_t (Fig. 17.1(b)), the inclusion of past measurements of Y_t in addition to that of X_t and Z_t results in better predictions of X_t , leading to $\Sigma_{xx} < \Sigma_3$, and $F_{Y \rightarrow X|Z} > 0$.

17.3.2 Frequency Domain Formulation

To derive the spectral decomposition of the time domain conditional Granger causality we carry out a normalization procedure like that for the bivariate case. For Eq. (17.30) and Eq. (17.31) the normalized equations are

$$\begin{pmatrix} D_{11}(L) & D_{12}(L) \\ D_{21}(L) & D_{22}(L) \end{pmatrix} \begin{pmatrix} x_t \\ z_t \end{pmatrix} = \begin{pmatrix} x_t^* \\ z_t^* \end{pmatrix}, \quad (17.37)$$

where $D_{11}(0) = 1$, $D_{22}(0) = 1$, $D_{12}(0) = 0$, $\text{cov}(x_t^*, z_t^*) = 0$, and $D_{21}(0)$ is generally not zero. We note that $\text{var}(x_t^*) = \Sigma_3$ and this becomes useful in what follows.

For Eqs. (17.33), (17.34), and (17.35) the normalization process involves left-multiplying both sides by the matrix

$$P = P_2 \cdot P_1 \quad (17.38)$$

where

$$P_1 = \begin{pmatrix} 1 & 0 & 0 \\ -\Sigma_{yx}\Sigma_{xx}^{-1} & 1 & 0 \\ -\Sigma_{zx}\Sigma_{xx}^{-1} & 0 & 1 \end{pmatrix}, \quad (17.39)$$

and

$$P_2 = \begin{pmatrix} 1 & 0 & 0 \\ 0 & 1 & 0 \\ 0 & -(\Sigma_{zy} - \Sigma_{zx}\Sigma_{xx}^{-1}\Sigma_{xy})(\Sigma_{yy} - \Sigma_{yx}\Sigma_{xx}^{-1}\Sigma_{xy})^{-1} & 1 \end{pmatrix}. \quad (17.40)$$

We denote the normalized equations as

$$\begin{pmatrix} B_{11}(L) & B_{12}(L) & B_{13}(L) \\ B_{21}(L) & B_{22}(L) & B_{23}(L) \\ B_{31}(L) & B_{32}(L) & B_{33}(L) \end{pmatrix} \begin{pmatrix} x_t \\ y_t \\ z_t \end{pmatrix} = \begin{pmatrix} \epsilon_{xt} \\ \epsilon_{yt} \\ \epsilon_{zt} \end{pmatrix}, \quad (17.41)$$

where the noise terms are independent, and their respective variances are $\hat{\Sigma}_{xx}$, $\hat{\Sigma}_{yy}$, and $\hat{\Sigma}_{zz}$.

To proceed further we need the following important relation [4]:

$$F_{Y \rightarrow X|Z} = F_{YZ^* \rightarrow X^*} \quad (17.42)$$

and its frequency domain counterpart

$$f_{Y \rightarrow X|Z}(\omega) = f_{YZ^* \rightarrow X^*}(\omega). \quad (17.43)$$

To obtain $f_{YZ^* \rightarrow X^*}(\omega)$, we need to decompose the spectrum of X^* . The Fourier transform of Eqs. (17.37) and (17.41) gives

$$\begin{pmatrix} X(\omega) \\ Z(\omega) \end{pmatrix} = \begin{pmatrix} G_{xx}(\omega) & G_{xz}(\omega) \\ G_{zx}(\omega) & G_{zz}(\omega) \end{pmatrix} \begin{pmatrix} X^*(\omega) \\ Z^*(\omega) \end{pmatrix}, \quad (17.44)$$

and

$$\begin{pmatrix} X(\omega) \\ Y(\omega) \\ Z(\omega) \end{pmatrix} = \begin{pmatrix} H_{xx}(\omega) & H_{xy}(\omega) & H_{xz}(\omega) \\ H_{yx}(\omega) & H_{yy}(\omega) & H_{yz}(\omega) \\ H_{zx}(\omega) & H_{zy}(\omega) & H_{zz}(\omega) \end{pmatrix} \begin{pmatrix} E_x(\omega) \\ E_y(\omega) \\ E_z(\omega) \end{pmatrix}. \quad (17.45)$$

Assuming that $X(\omega)$ and $Z(\omega)$ from Eq. (17.44) can be equated with that from Eq. (17.45), we combine Eqs. (17.44) and (17.45) to yield

$$\begin{pmatrix} X^*(\omega) \\ Y(\omega) \\ Z^*(\omega) \end{pmatrix} = \begin{pmatrix} G_{xx}(\omega) & 0 & G_{xz}(\omega) \\ 0 & 1 & 0 \\ G_{zx}(\omega) & 0 & G_{zz}(\omega) \end{pmatrix}^{-1} \begin{pmatrix} H_{xx}(\omega) & H_{xy}(\omega) & H_{xz}(\omega) \\ H_{yx}(\omega) & H_{yy}(\omega) & H_{yz}(\omega) \\ H_{zx}(\omega) & H_{zy}(\omega) & H_{zz}(\omega) \end{pmatrix} \begin{pmatrix} E_x(\omega) \\ E_y(\omega) \\ E_z(\omega) \end{pmatrix} \\ = \begin{pmatrix} Q_{xx}(\omega) & Q_{xy}(\omega) & Q_{xz}(\omega) \\ Q_{yx}(\omega) & Q_{yy}(\omega) & Q_{yz}(\omega) \\ Q_{zx}(\omega) & Q_{zy}(\omega) & Q_{zz}(\omega) \end{pmatrix} \begin{pmatrix} E_x(\omega) \\ E_y(\omega) \\ E_z(\omega) \end{pmatrix}, \quad (17.46)$$

where $Q(\omega) = G^{-1}(\omega)H(\omega)$. After suitable ensemble averaging, the spectral matrix can be obtained from which the power spectrum of X^* is found to be

$$S_{X^*X^*}(\omega) = Q_{xx}(\omega)\hat{\Sigma}_{xx}Q_{xx}^*(\omega) + Q_{xy}(\omega)\hat{\Sigma}_{yy}Q_{xy}^*(\omega) + Q_{xz}(\omega)\hat{\Sigma}_{zz}Q_{xz}^*(\omega). \quad (17.47)$$

The
tern
imn

We
the
from

It ca

unde
I
and
pure
syste
satis
tion
of co

17.4

The
well
proce
gress
ratio
consi
neuro
for th
cond
as rec
L
notes
numb
be de

The first term can be thought of as the intrinsic power and the remaining two terms as the combined causal influences from Y to Z^* . This interpretation leads immediately to the definition

$$f_{YZ^* \rightarrow X^*}(\omega) = \ln \frac{|S_{X^*X^*}(\omega)|}{|Q_{XX}(\omega) \hat{\Sigma}_{XX} Q_{XX}^*(\omega)|} \quad (17.48)$$

We note that $S_{X^*X^*}(\omega)$ is actually the variance of ϵ_{3t} as pointed out earlier. On the basis of the relation in Eq. (17.43), the final expression for Granger causality from Y_t to X_t conditional on Z_t is

$$f_{Y \rightarrow X|Z}(\omega) = \ln \frac{\Sigma_3}{|Q_{XX}(\omega) \hat{\Sigma}_{XX} Q_{XX}^*(\omega)|} \quad (17.49)$$

It can be shown that $f_{Y \rightarrow X|Z}(\omega)$ relates to the time domain measure $F_{Y \rightarrow X|Z}$ via

$$F_{Y \rightarrow X|Z} = \frac{1}{2\pi} \int_{-\pi}^{\pi} f_{Y \rightarrow X|Z}(\omega) d\omega,$$

under general conditions.

The above derivation is made possible by the key assumption that $X(\omega)$ and $Z(\omega)$ in Eqs. (17.44) and (17.45) are identical. This certainly holds true on purely theoretical grounds, and it may very well be true for simple mathematical systems. For actual physical data, however, this condition may be very hard to satisfy due to practical estimation errors. In a recent paper we developed a partition matrix technique to overcome this problem [6]. The subsequent calculations of conditional Granger causality are based on this partition matrix procedure.

17.4 Estimation of Autoregressive Models

The preceding theoretical development assumes that the time series can be well represented by autoregressive processes. Such theoretical autoregressive processes have infinite model orders. Here we discuss how to estimate autoregressive models from empirical time series data, with emphasis on the incorporation of multiple time series segments into the estimation procedure [7]. This consideration is motivated by the goal of applying autoregressive modeling in neuroscience. It is typical in behavioral and cognitive neuroscience experiments for the same event to be repeated on many successive trials. Under appropriate conditions, time series data recorded from these repeated trials may be viewed as realizations of a common underlying stochastic process.

Let $X_t = [X_{1t}, X_{2t}, \dots, X_{pt}]^T$ be a p -dimensional random process. Here T denotes the matrix transposition. In multivariate neural data, p represents the total number of recording channels. Assume that the process X_t is stationary and can be described by the following m th order autoregressive equation:

$$X_t + A(1)X_{t-1} + \dots + A(m)X_{t-m} = E_t, \quad (17.50)$$

where $\mathbf{A}(i)$ are $p \times p$ coefficient matrices and $\mathbf{E}_t = [E_{1t}, E_{2t}, \dots, E_{pt}]^T$ is a zero mean uncorrelated noise vector with the covariance matrix Σ .

To estimate $\mathbf{A}(i)$ and Σ , we multiply Eq. (17.50) from the right by \mathbf{X}_{t-k}^T , where $k = 1, 2, \dots, m$. Taking expectations, we obtain the Yule-Walker equations

$$\mathbf{R}(-k) + \mathbf{A}(1)\mathbf{R}(-k+1) + \dots + \mathbf{A}(m)\mathbf{R}(-k+m) = \mathbf{0}, \quad (17.51)$$

where $\mathbf{R}(n) = \langle \mathbf{X}_t \mathbf{X}_{t+n}^T \rangle$ is \mathbf{X}_t 's covariance matrix of lag n . In deriving these equations, we have used the fact that $\langle \mathbf{E}_t \mathbf{X}_{t-k}^T \rangle = \mathbf{0}$ as a result of \mathbf{E}_t being an uncorrelated process.

For a single realization of the \mathbf{X} process, $\{x_i\}_{i=1}^N$, we compute the covariance matrix in Eq. (17.51) according to

$$\tilde{\mathbf{R}}(n) = \frac{1}{N-n} \sum_{i=1}^{N-n} x_i x_{i+n}^T. \quad (17.52)$$

If multiple realizations of the same process are available, then we compute the above quantity for each realization, and average across all the realizations to obtain the final estimate of the covariance matrix. Note that for a single short trial of data one uses the divisor N for evaluating covariance to reduce inconsistency. Due to the availability of multiple trials in neural applications, we have used the divisor $(N - n)$ in the above definition, Eq. (17.52), to achieve an unbiased estimate. It is quite clear that, for a single realization, if N is small, one will not get good estimates of $\mathbf{R}(n)$ and hence will not be able to obtain a good model. This problem can be overcome if a large number of realizations of the same process is available. In this case the length of each realization can be as short as the model order m plus 1. Equation (17.50) contain a total of mp^2 unknown model coefficients. In Eq. (17.51) there is exactly the same number of simultaneous linear equations. One can simply solve these equations to obtain the model coefficients. An alternative approach is to use the Levinson, Wiggins, Robinson (LWR) algorithm, which is a more robust solution procedure based on the ideas of maximum entropy. This algorithm was implemented in the analysis of neural data described below. The noise covariance matrix Σ may be obtained as part of the LWR algorithm. Otherwise one may obtain Σ through

$$\Sigma = \mathbf{R}(0) + \sum_{i=1}^m \mathbf{A}(i)\mathbf{R}(i). \quad (17.53)$$

Here we note that $\mathbf{R}^T(k) = \mathbf{R}(-k)$.

The above estimation procedure can be carried out for any model order m . The correct m is usually determined by minimizing the Akaike Information Criterion (AIC) defined as

$$\text{AIC}(m) = 2 \log[\det(\Sigma)] + \frac{2p^2 m}{N_{\text{total}}} \quad (17.54)$$

where N_{total} is the total number of data points from all the trials. Plotted as a function of m the proper model order corresponds to the minimum of this function. It is often the case that for neurobiological data N_{total} is very large. Consequently, for a reasonable range of m , the AIC function does not achieve a minimum. An alternative criterion is the Bayesian Information Criterion (BIC), which is defined as

$$\text{BIC}(m) = 2 \log[\det(\Sigma)] + \frac{2p^2 m \log N_{\text{total}}}{N_{\text{total}}}. \quad (17.55)$$

This criterion can compensate for the large number of data points and may perform better in neural applications. A final step, necessary for determining whether the autoregressive time series model is suited for a given data set, is to check whether the residual noise is white. Here the residual noise is obtained by computing the difference between the model's predicted values and the actually measured values.

Once an autoregressive model is adequately estimated, it becomes the basis for both time domain and spectral domain causality analysis. Specifically, in the spectral domain, Eq. (17.50) can be written as

$$\mathbf{X}(\omega) = \mathbf{H}(\omega)\mathbf{E}(\omega), \quad (17.56)$$

where

$$\mathbf{H}(\omega) = \left(\sum_{j=0}^m \mathbf{A}(j)e^{-i\omega j} \right)^{-1} \quad (17.57)$$

is the transfer function with $\mathbf{A}(0)$ being the identity matrix. From Eq. (17.56), after proper ensemble averaging, we obtain the spectral matrix

$$\mathbf{S}(\omega) = \mathbf{H}(\omega)\Sigma\mathbf{H}^*(\omega). \quad (17.58)$$

Once we obtain the transfer function, the noise covariance, and the spectral matrix, we can then carry out causality analysis according to the procedures outlined in the previous sections.

17.5 Numerical Examples

In this section we consider three examples that illustrate various aspects of the general approach outlined earlier.

17.5.1 Example 1

Consider the following AR(2) model

$$\begin{aligned} X_t &= 0.9X_{t-1} - 0.5X_{t-2} + \epsilon_t \\ Y_t &= 0.8Y_{t-1} - 0.5Y_{t-2} + 0.16X_{t-1} - 0.2X_{t-2} + \eta_t \end{aligned} \quad (17.59)$$

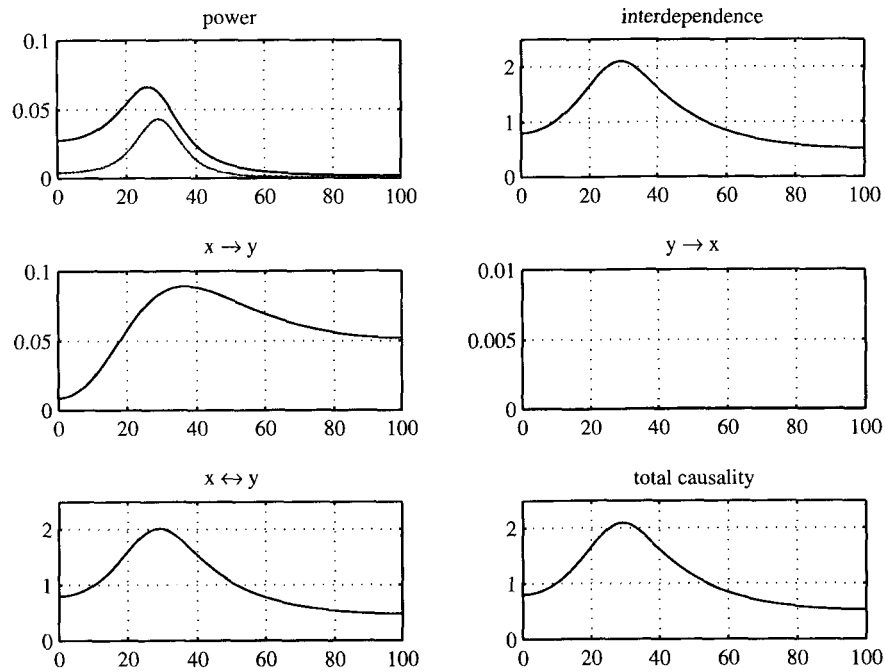


Fig. 17.2: Simulation results for an AR(2) model consisting of two coupled time series. Power (black for X , gray for Y) spectra, interdependence spectrum (related to the coherence spectrum), and Granger causality spectra are displayed. Note that the total causality spectrum, representing the sum of directional causalities and the instantaneous causality, is nearly identical to the interdependence spectrum.

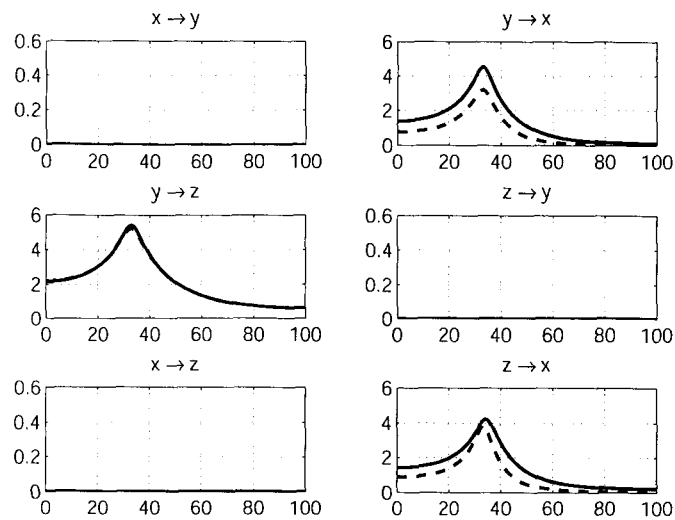
where ϵ_t, η_t are Gaussian white noise processes with zero means and variances $\sigma_1^2 = 1, \sigma_2^2 = 0.7$, respectively. The covariance between ϵ_t and η_t is 0.4. From the construction of the model, we can see that X_t has a causal influence on Y_t and that there is also instantaneous causality between X_t and Y_t .

We simulated Eq. (17.59) to generate a data set of 500 realizations of 100 time points each. Assuming no knowledge of Eq. (17.59) we fitted a MVAR model on the generated data set and calculated power, coherence, and Granger causality spectra. The result is shown in Fig. 17.2. The interdependence spectrum is computed according to Eq. (17.17) and the total causality is defined as the sum of directional causalities and the instantaneous causality. The result clearly recovers the pattern of connectivity in Eq. (17.59). It also illustrates that the interdependence spectrum, as computed according to Eq. (17.17), is almost identical to the total causality spectrum as defined on the right-hand side of Eq. (17.28).

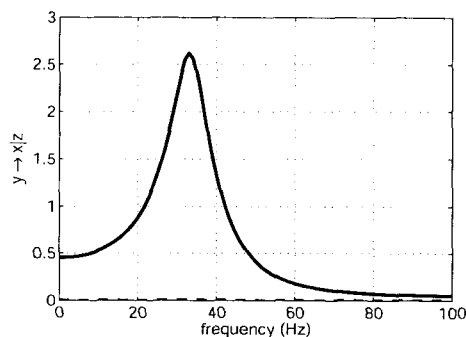
F
o
w
w
c
p
d
a

17.5.2

Here w
the cas
indirect



(a)



(b)

Fig. 17.3: Simulation results for three coupled time series. Two distinct patterns of connectivity as that illustrated in Fig. 17.1 are considered. Results for the case with a direct causal influence are shown as solid curves and the results for the case with indirect causal influence are shown as dashed curves. (a) Pairwise Granger causality analysis gives very similar results for both cases which indicates that the pairwise analysis cannot differentiate these two patterns of connectivity. (b) Conditional causality analysis shows a nonzero spectrum (solid) for the direct case and almost zero spectrum (dashed) for the indirect case.

17.5.2 Example 2

Here we consider two models. The first consists of three time series simulating the case shown in Fig. 17.1(a), in which the causal influence from Y_t to X_t is indirect and completely mediated by Z_t

$$\begin{aligned}
 X_t &= 0.8X_{t-1} - 0.5X_{t-2} + 0.4Z_{t-1} + \epsilon_t \\
 Y_t &= 0.9Y_{t-1} - 0.8Y_{t-2} + \xi_t \\
 Z_t &= 0.5Z_{t-1} - 0.2Z_{t-2} + 0.5Y_{t-1} + \eta_t .
 \end{aligned}
 \tag{17.60}$$

The second model creates a situation corresponding to Fig. 17.1(b), containing both direct and indirect causal influences from Y_t to X_t . This is achieved by using the same system as in Eq. (17.60), but with an additional term in the first equation

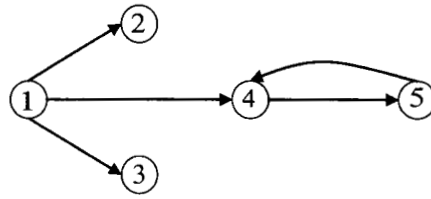
$$\begin{aligned}
 X_t &= 0.8X_{t-1} - 0.5X_{t-2} + 0.4Z_{t-1} + 0.2Y_{t-2} + \epsilon_t \\
 Y_t &= 0.9Y_{t-1} - 0.8Y_{t-2} + \xi_t \\
 Z_t &= 0.5Z_{t-1} - 0.2Z_{t-2} + 0.5Y_{t-1} + \eta_t .
 \end{aligned}
 \tag{17.61}$$

For both models, $\epsilon(t)$, $\xi(t)$, $\eta(t)$ are three independent Gaussian white noise processes with zero means and variances of $\sigma_1^2 = 0.3$, $\sigma_2^2 = 1$, $\sigma_3^2 = 0.2$, respectively.

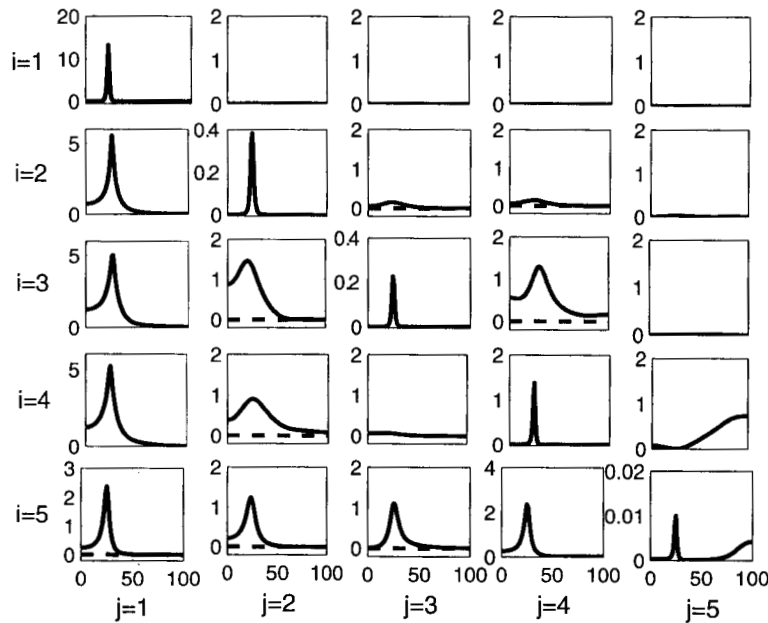
Each model was simulated to generate a data set of 500 realizations of 100 time points each. First, pairwise Granger causality analysis was performed on the simulated data set of each model. The results are shown in Fig. 17.3(a), with the dashed curves showing the results for the first model and the solid curves for the second model. From these plots it is clear that pairwise analysis cannot differentiate the two coupling schemes. This problem occurs because the indirect causal influence from Y_t to X_t that depends completely on Z_t in the first model cannot be clearly distinguished from the direct influence from Y_t to X_t in the second model. Next, conditional Granger causality analysis was performed on both simulated data sets. The Granger causality spectra from Y_t to X_t conditional on Z_t are shown in Fig. 17.3(b), with the second model's result shown as the solid curve and the first model's result as the dashed curve. Clearly, the causal influence from Y_t to X_t that was prominent in the pairwise analysis of the first model in Fig. 17.3(a), is no longer present in Fig. 17.3(b). Thus, by correctly determining that there is no direct causal influence from Y_t to X_t in the first model, the conditional Granger causality analysis provides an unambiguous dissociation of the coupling schemes represented by the two models.

17.5.3 Example 3

We simulated a five-node oscillatory network structurally connected with different delays. This example has been analyzed with partial directed coherence and directed transfer function methods in [8]. The network involves the following multivariate autoregressive model:



(a)



(b)

Fig. 17.4: Simulation results for a five-node network structurally connected with different time delays. (a) Schematic illustration of the system. (b) Calculated power spectra are shown in the diagonal panels, results of pairwise (solid) and conditional Granger causality analysis (dashed) are in off-diagonal panels. Granger causal influence is from the horizontal index to the vertical index. Features of Granger causality spectra (both pairwise and conditional) are consistent with that of power spectra.

$$\begin{aligned}
 X_{1t} &= 0.95\sqrt{2}X_{1(t-1)} - 0.9025X_{1(t-2)} + \epsilon_{1t} \\
 X_{2t} &= 0.5X_{1(t-2)} + \epsilon_{2t} \\
 X_{3t} &= -0.4X_{1(t-3)} + \epsilon_{3t} \\
 X_{4t} &= -0.5X_{1(t-2)} + 0.25\sqrt{2}X_{4(t-1)} + 0.25\sqrt{2}X_{5(t-1)} + \epsilon_{4t} \\
 X_{5t} &= -0.25\sqrt{2}X_{4(t-1)} + 0.25\sqrt{2}X_{5(t-1)} + \epsilon_{5t},
 \end{aligned}
 \tag{17.62}$$

where $\epsilon_{1t}, \epsilon_{2t}, \epsilon_{3t}, \epsilon_{4t}, \epsilon_{5t}$ are independent Gaussian white noise processes with zero means and variances of $\sigma_1^2 = 0.6$, $\sigma_2^2 = 0.5$, $\sigma_3^2 = 0.3$, $\sigma_4^2 = 0.3$, $\sigma_5^2 = 0.6$, respectively. The structure of the network is illustrated in Fig. 17.4(a).

We simulated the network model to generate a data set of 500 realizations each with ten time points. Assuming no knowledge of the model, we fitted a fifth order MVAR model on the generated data set and performed power spectra, coherence, and Granger causality analysis on the fitted model. The results of power spectra are given in the diagonal panels of Fig. 17.4(b). It is clearly seen that all five oscillators have a spectral peak at around 25 Hz and the fifth has some additional high frequency activity as well. The results of pairwise Granger causality spectra are shown in the off-diagonal panels of Fig. 17.4(b) (solid curves). Compared to the network diagram in Fig. 17.4(a) we can see that pairwise analysis yields connections that can be the result of direct causal influences (e.g., $1 \rightarrow 2$), indirect causal influences (e.g., $1 \rightarrow 5$) and differentially delayed driving inputs (e.g., $2 \rightarrow 3$). We further performed a conditional Granger causality analysis in which the direct causal influence between any two nodes are examined while the influences from the other three nodes are conditioned out. The results are shown as dashed curves in Fig. 17.4(b). For many pairs the dashed curves and solid curves coincide (e.g., $1 \rightarrow 2$), indicating that the underlying causal influence is direct. For other pairs the dashed curves become zero, indicating that the causal influences in these pairs are either indirect or are the result of differentially delayed inputs. These results demonstrate that conditional Granger causality furnishes a more precise network connectivity diagram that matches the known structural connectivity. One noteworthy feature about Fig. 17.4(b) is that the spectral features (e.g., peak frequency) are consistent across both power and Granger causality spectra. This is important since it allows us to link local dynamics with that of the network.

17.6 Analysis of a Beta Oscillation Network in Sensorimotor Cortex

A number of studies have appeared in the neuroscience literature where the issue of causal effects in neural data is examined [6, 8–15]. Three of these studies [10, 11, 15] used the measures presented in this article. Below we review one study published by our group [6, 15].

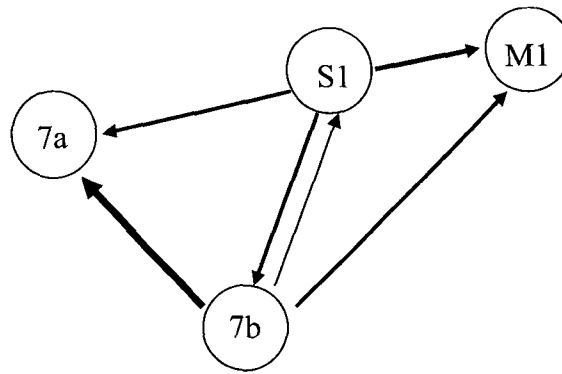
Local field potential data were recorded from two macaque monkeys using transcortical bipolar electrodes at 15 distributed sites in multiple cortical areas of one hemisphere (the right hemisphere in monkey GE and the left hemisphere in monkey LU) while the monkeys performed a GO/NO-GO visual pattern discrimination task [16]. The prestimulus stage began when the monkey depressed a hand lever while monitoring a display screen. This was followed from 0.5 s to 1.25 s later by the appearance of a visual stimulus (a four-dot pattern) on the screen. The monkey made a GO response (releasing the lever) or a NO-GO re-

sponse (maintaining lever depression) depending on the stimulus category and the session contingency. The entire trial lasted about 500 ms, during which the local field potentials were recorded at a sampling rate of 200 Hz.

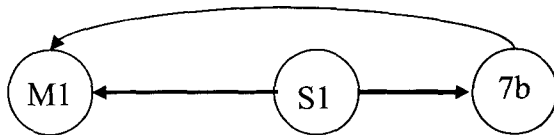
Previous studies have shown that synchronized beta-frequency (15 Hz to 30 Hz) oscillations in the primary motor cortex are involved in maintaining steady contractions of contralateral arm and hand muscles. Relatively little is known, however, about the role of postcentral cortical areas in motor maintenance and their patterns of interaction with motor cortex. Making use of the simultaneous recordings from distributed cortical sites we investigated the interdependency relations of beta-synchronized neuronal assemblies in pre- and postcentral areas in the prestimulus time period. Using power and coherence spectral analysis, we first identified a beta-synchronized large-scale network linking pre- and postcentral areas. We then used Granger causality spectra to measure directional influences among recording sites, ascertaining that the dominant causal influences occurred in the same part of the beta-frequency range as indicated by the power and coherence analysis. The patterns of significant beta-frequency Granger causality are summarized in the schematic Granger causality graphs shown in Fig. 17.5. These patterns reveal that, for both monkeys, strong Granger causal influences occurred from the primary somatosensory cortex (S1) to both the primary motor cortex (M1) and inferior posterior parietal cortex (7a and 7b), with the latter areas also exerting Granger causal influences on the primary motor cortex. Granger causal influences from the motor cortex to postcentral areas, however, were not observed.²

Our results are the first to demonstrate in awake monkeys that synchronized beta oscillations not only bind multiple sensorimotor areas into a large-scale network during motor maintenance behavior, but also carry Granger causal influences from primary somatosensory and inferior posterior parietal cortices to motor cortex. Furthermore, the Granger causality graphs in Fig. 17.5 provide a basis for fruitful speculation about the functional role of each cortical area in the sensorimotor network. First, steady pressure maintenance is akin to a closed-loop-control problem and as such, sensory feedback is expected to provide critical input needed for cortical assessment of the current state of the behavior. This notion is consistent with our observation that primary somatosensory area (S1) serves as the dominant source of causal influences to other areas in the network. Second, posterior parietal area 7b is known to be involved in non-visually guided movement. As a higher-order association area it may maintain representations relating to the current goals of the motor system. This would imply that area 7b receives sensory updates from area S1 and outputs correctional signals to the motor cortex (M1). This conceptualization is consistent with the causality patterns in Fig. 17.5. As mentioned earlier, previous work has identified beta range oscillations in the motor cortex as an important neural correlate of

² A more stringent significance threshold was applied here which resulted in elimination of several very small causal influences that were included in the previous report.



(a)



(b)

Fig. 17.5: Granger causality graphs for monkey GE (a) and monkey LU (b).

pressure maintenance behavior. The main contribution of our work is to demonstrate that the beta network exists on a much larger scale and that postcentral areas play a key role in organizing the dynamics of the cortical network. The latter conclusion is made possible by the directional information provided by Granger causality analysis.

Since the above analysis was pairwise, it had the disadvantage of not distinguishing between direct and indirect causal influences. In particular, in monkey GE, the possibility existed that the causal influence from area S1 to inferior posterior parietal area 7a was actually mediated by inferior posterior parietal area 7b (Fig. 17.5(a)). We used the conditional Granger causality to test the hypothesis that the $S1 \rightarrow 7a$ influence was mediated by area 7b. In Fig. 17.6(a) is presented the pairwise Granger causality spectrum from S1 to 7a ($S1 \rightarrow 7a$, dark solid curve), showing significant causal influence in the beta-frequency range. Superimposed in Fig. 17.6(a) is the conditional Granger causality spectrum for the same pair, but with area 7b taken into account ($S1 \rightarrow 7a | 7b$, light solid curve). The corresponding 99% significance thresholds are also presented (light and dark dashed lines coincide). These significance thresholds were determined using a

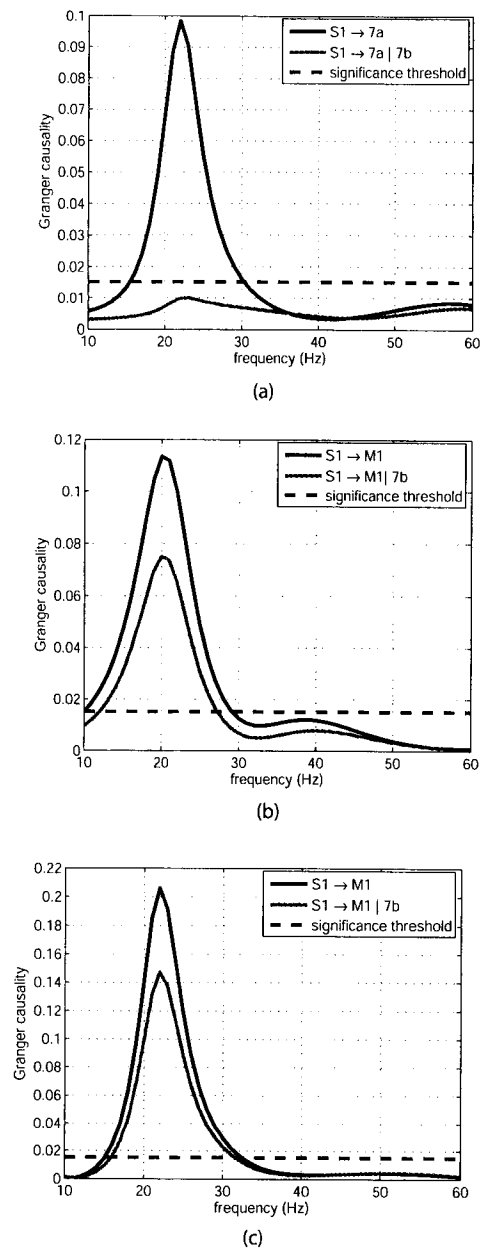


Fig. 17.6: Comparison of pairwise and conditional Granger causality spectra for monkey GE (a,b), and monkey LU (c).

permutation procedure that involved creating 500 permutations of the local field potential data set by random rearrangement of the trial order independently for each channel (site). Since the test was performed separately for each frequency, a correction was necessary for the multiple comparisons over the whole range of frequencies. The Bonferroni correction could not be employed because these multiple comparisons were not independent. An alternative strategy was employed following Blair and Karniski [17]. The Granger causality spectrum was computed for each permutation, and then the maximum causality value over the frequency range was identified. After 500 permutation steps, a distribution of maximum causality values was created. Choosing a p-value at $p = 0.01$ for this distribution gave the thresholds shown in Fig. 17.6(a)–(c) as the dashed lines.

We see from Fig. 17.6(a) that the conditional Granger causality is greatly reduced in the beta-frequency range and no longer significant, meaning that the causal influence from S1 to 7a is most likely an indirect effect mediated by 7b. This conclusion is consistent with the known neuroanatomy of the sensorimotor cortex [18] in which area 7a receives direct projections from area 7b which in turn receives direct projections from the primary somatosensory cortex. No pathway is known to project directly from the primary somatosensory cortex to area 7a.

From Fig. 17.5(a) we see that the possibility also existed that the causal influence from S1 to the primary motor cortex (M1) in monkey GE was mediated by area 7b. To test this possibility, the Granger causality spectrum from S1 to M1 ($S1 \rightarrow M1$, dark solid curve in Fig. 17.6(b)) was compared with the conditional Granger causality spectrum with 7b taken into account ($S1 \rightarrow M1 | 7b$, light solid curve in Fig. 17.6(b)). In contrast to Fig. 17.6(a), we see that the beta-frequency conditional Granger causality in Fig. 17.6(b) is only partially reduced, and remains well above the 99% significance level. From Fig. 17.4(b), we see that the same possibility existed in monkey LU of the S1 to M1 causal influence being mediated by 7b. However, just as in Fig. 17.6(b), we see in Fig. 17.6(c) that the beta-frequency conditional Granger causality for monkey LU is only partially reduced, and remains well above the 99% significance level.

The results from both the monkeys thus indicate that the observed Granger causal influence from the primary somatosensory cortex to the primary motor cortex was not simply an indirect effect mediated by area 7b. However, we further found that area 7b did play a role in mediating the S1 to M1 causal influence in both the monkeys. This was determined by comparing the means of bootstrap resampled distributions of the peak beta Granger causality values from the spectra of $S1 \rightarrow M1$ and $S1 \rightarrow M1 | 7b$ by the Student's t-test. The significant reduction of beta-frequency Granger causality when area 7b is taken into account ($t = 17.2$ for GE; $t = 18.2$ for LU, $p \ll 0.001$ for both), indicates that the influence from the primary somatosensory to primary motor area was partially mediated by area 7b. Such an influence is consistent with the known neuroanatomy [18] where the primary somatosensory area projects directly to both the motor cortex and area 7b, and area 7b projects directly to primary motor cortex.

17.7 Summary

In this chapter we have introduced the mathematical formalism for estimating Granger causality in both the time and spectral domain from time series data. Demonstrations of the technique's utilities are carried out both on simulated data, where the patterns of interactions are known, and on local field potential recordings from monkeys performing a cognitive task. For the latter we have stressed the physiological interpretability of the findings and pointed out the new insights afforded by these findings. It is our belief that Granger causality offers a new way of looking at cooperative neural computation and it enhances our ability to identify key brain structures underlying the organization of a given brain function.

Acknowledgements

This work was supported by NIMH grant MH071620.

References

- [1] N. Wiener. The theory of prediction. In E. F. Beckenbach, editor, *Modern Mathematics for Engineers*, chap. 8. McGraw-Hill, New York, 1956.
- [2] C. W. J. Granger. *Econometrica*, 37:424, 1969.
- [3] J. Geweke. *J. Am. Stat. Assoc.*, 77:304, 1982.
- [4] J. Geweke. *J. Am. Stat. Assoc.*, 79:907, 1984.
- [5] C. Gourierous and A. Monfort. *Time Series and Dynamic Models*. Cambridge University Press, London, 1997.
- [6] Y. Chen, S. L. Bressler, and M. Ding. *J. Neurosci. Methods*, 150:228, 2006.
- [7] M. Ding, S. L. Bressler, W. Yang, and H. Liang. *Biol. Cybern.*, 83:35, 2000.
- [8] L. A. Baccala and K. Sameshima. *Biol. Cybern.*, 84:463, 2001.
- [9] W. A. Freiwald, P. Valdes, J. Bosch, et al. *J. Neurosci. Methods*, 94:105, 1999.
- [10] C. Bernasconi and P. Konig. *Biol. Cybern.*, 81:199, 1999.
- [11] C. Bernasconi, A. von Stein, C. Chiang, and P. Konig. *Neuroreport*, 11:689, 2000.
- [12] M. Kaminski, M. Ding, W. A. Truccolo, and S. L. Bressler. *Biol. Cybern.*, 85: 145, 2001.
- [13] R. Goebel, A. Roebroek, D. Kim, and E. Formisano. *Magn. Res. Imag.*, 21: 1251, 2003.

- [14] W. Hesse, E. Moller, M. Arnold, and B. Schack. *J. Neurosci. Methods*, 124:27, 2003.
- [15] A. Brovelli, M. Ding, A. Ledberg, Y. Chen, R. Nakamura, and S. L. Bressler. *Proc. Natl. Acad. Sci.*, 101:9849, 2004.
- [16] S. L. Bressler, R. Coppola, and R. Nakamura. *Nature*, 366:153, 1993.
- [17] R. C. Blair and W. Karniski. *Psychophysiol.*, 30:518, 1993.
- [18] D. J. Felleman and D. C. V. Essen. *Cereb. Cortex*, 1:1, 1991.

1

Pe
LeTh
ali
un
Gr
tia
ser
tin
vol
art
ter
ato
app
tw
ust
fiel
ma
sm
ger
lect
pai
clu
pai
ple
firs
gen
tim
sim
use
date
of tlHandl
Copy
ISBN: